Journal of
Water & Climate Change

IWA PUBLISHING

Journal of Water and Climate Change Vol 16 No 10, 3178 doi: 10.2166/wcc.2025.139

Impacts of climate change on the water budget elements in the Faria catchment, Palestine

Qais Daraghma[a] and Abdelhaleem Khader[b,*]

[a] Faculty of Graduate Studies, An-Najah National University, Nablus P4110257, Palestine
[b] Department of Civil Engineering, An-Najah National University, Nablus P4110257, Palestine
*Corresponding author. E-mail: a.khader@najah.edu

AK, 0000-0003-4710-1362

ABSTRACT

This study assesses the impacts of climate change on water budget components in the semi-arid Faria catchment, Palestine. Using climate projections from SimClim AR6 under the SSP2-4.5 and SSP5-8.5 scenarios and hydrological modeling via the Soil and Water Assessment Tool, the research evaluates changes in precipitation, temperature, humidity, wind speed, and solar radiation for the years 2060 and 2100. Calibration and validation show good model performance ($R^2 = 0.67$, NSE = 0.64). Results reveal declining precipitation and relative humidity, with groundwater recharge expected to drop by up to 27.43% and surface runoff by up to 43.31% by 2100. Simultaneously, rising temperatures lead to higher evapotranspiration, reaching a 9.64% increase under the SSP5-8.5 scenario. These shifts result in a significant decrease in overall water yield, posing a threat to water security in the region. The study highlights the urgent need for adaptive water management strategies and promotes the use of integrated climate-hydrological modeling for sustainability planning in similar semi-arid catchments.

Key words: climate change, semi-arid zones, SimClim AR6, state of Palestine, SWAT model, watershed hydrology

HIGHLIGHTS

- Integrated SimClim AR6 and SWAT for climate-hydrology modeling in semi-arid regions.
- The first study to assess climate change impacts on water budget in the Faria catchment, Palestine.
- Projects significant reductions in runoff and groundwater recharge under the SSP scenarios.
- Provides actionable insights for water resource adaptation in arid zones.
- Uses 23-GCM ensemble for robust local forecasting.

GRAPHICAL ABSTRACT

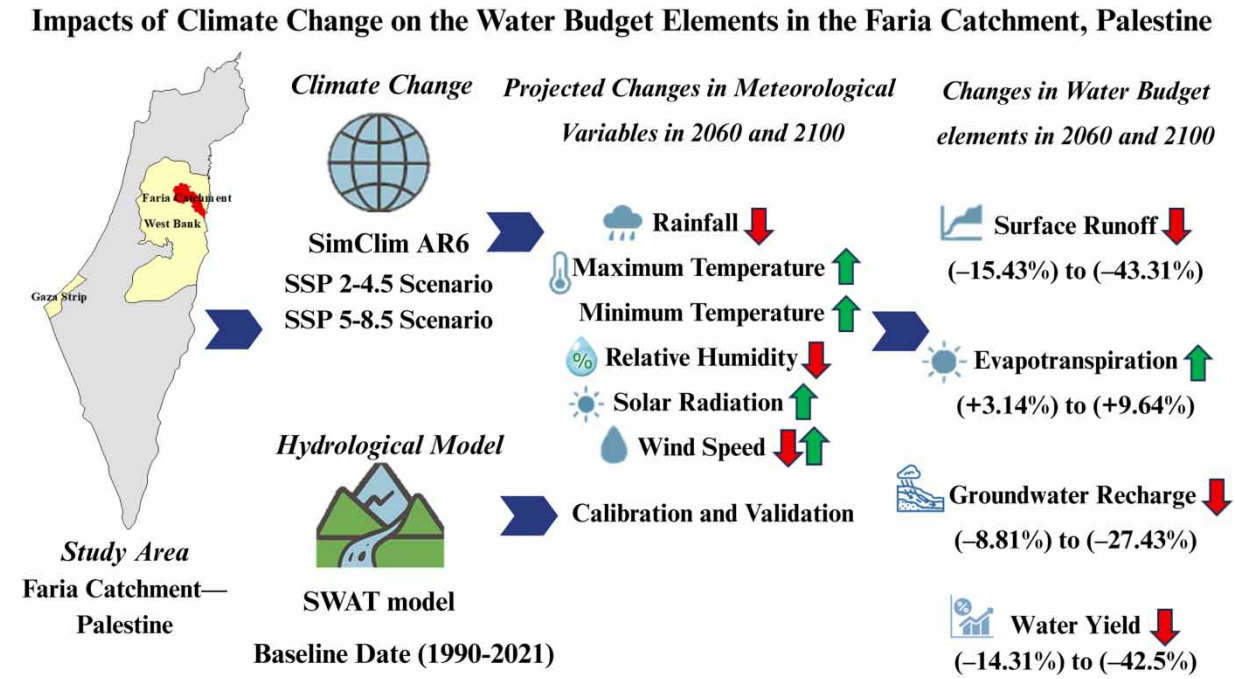

1. INTRODUCTION

Water stands as one of life's most vital components and a cornerstone of societal prosperity (Gleick 1998). This essential resource underpins human existence and diverse activities (Falkenmark & Rockström 2006), yet rapidly expanding populations and evolving living needs intensify daily demand (Vörösmarty *et al.* 2000). Preserving water sources and optimizing utilization is therefore imperative to cover all needs (Hoekstra & Mekonnen 2012).

Climate, defined as average weather conditions over months to millennia (Schneider & Novak 2023), faces unprecedented disruption from greenhouse gas emissions and human activities (e.g., industrialization, urbanization, land-use changes) (IPCC 2014). The IPCC AR6 report quantifies this crisis; global surface temperatures in 2011–2020 exceeded 1850–1900 levels by 1.09 °C (0.95–1.20 °C), with land warming of 1.59 °C (1.34–1.83 °C) (Masson-Delmotte *et al.* 2021). Such changes profoundly destabilize the hydrological cycle, amplifying extreme events (droughts, storms, reduced rainy days) and altering runoff patterns. Studying these impacts is critical for water sustainability (Mata *et al*. 2007).

Accurate streamflow analysis remains fundamental to catchment management, enabling flood forecasting, water allocation, and ecosystem protection in semi-arid regions (Vörösmarty *et al.* 2000). However, streamflow observations alone fail to reveal basin-scale water partitioning. Quantifying surface runoff (SRO), evapotranspiration (ET), and groundwater recharge is essential for actionable insights into sustainable resource allocation (Falkenmark & Rockström 2006). This is especially urgent in agricultural lands like the Faria catchment, as it is a key zone of the Jordan Valley, which is widely regarded as the food basket of the West Bank, supplying much of its primary agricultural produce (Shadeed *et al.* 2017). Decomposing the water budget into core fluxes allows precise targeting of interventions (e.g., optimized irrigation, managed aquifer recharge) (Hoekstra & Mekonnen 2012).

Hydrological modeling has evolved from lumped conceptual approaches to distributed process-based frameworks (Arnold *et al.* 1998). The Soil and Water Assessment Tool (SWAT) uniquely integrates climate, land use, soil, and management variables within a physically based structure (Neitsch *et al.* 2011). Its modular design, open-source support, and validation across semi-arid catchments make it ideal for the Faria catchment (Arnold *et al.* 2012). Crucially, SWAT simulates key meteorological variables beyond rainfall, such as solar radiation, humidity, wind speed, and temperature, enhancing energy-mass balance representation in irrigated systems (Santhi *et al*. 2001).

Prior hydrological study in the Faria catchment relied predominantly on HEC-HMS for streamflow estimation (Sulaiman 2017). However, critical gaps persist as there are no climate projections to assess future water budget elements. This void

obscures how shifting climate regimes will impact individual hydrological fluxes, thereby undermining agricultural resilience and water security.

The research has three main objectives:

Firstly, it investigates the impact of climate change on the meteorological variables in the Faria catchment for 2060 and 2100 based on the Shared Socioeconomic Pathways (SSPs) using the SimClim AR6 model (Abboushi 2013).

Secondly, it represents the modeling of the hydrological cycle in the Faria catchment using the SWAT to analyze the impact of climate change on water budget elements such as runoff, evaporation, and groundwater recharge based on the baseline daily data (1990–2021) (Arnold *et al.* 1998).

Finally, the study represents the amounts of the SRO, ET, and the amount of groundwater recharge from the rainfall on the Faria catchment for 2060 and 2100 under the climate scenarios. These objectives aim to understand the impact of climate change on the water budget elements in the Faria catchment.

This study adopts a hydroclimatic disturbance framework that conceptualizes the linkage between changes in climatic drivers (rainfall, temperature, humidity, solar radiation, and wind speed) and the redistribution of water within the catchment's hydrological system. The framework integrates future climate projections generated by the SimClim AR6 platform, which incorporates internal downscaling and bias adjustment of an ensemble of global climate models, under two greenhouse gas emission scenarios (SSP2-4.5 and SSP5-8.5) for two future time horizons (2060 and 2100). These climate inputs are incorporated into the SWAT2012 distributed hydrological model, configured with detailed spatial and climatic datasets representing the characteristics of the Faria catchment, to simulate key water budget components, namely SRO, ET, water yield (WY), and groundwater recharge. By combining climate projection tools with a physically based hydrological model, this framework provides an integrated approach for assessing how future climate change may alter the water balance in semi-arid catchments and supports the development of more sustainable water management strategies under anticipated climatic pressures.

It is hypothesized that rising temperatures and declining rainfall will non-linearly reduce key water budget components, particularly groundwater recharge, in semi-arid catchments. This response is expected to emerge from compounded impacts of reduced soil moisture, diminished infiltration, and intensified evaporative demand, especially under high-emission pathways. By integrating climate projection tools with a distributed hydrological model, this study aims to provide spatially explicit insights to support sustainable water resource management in vulnerable agricultural regions.

2. MATERIALS AND METHODS

2.1. Study area

The Faria catchment is located in the north-eastern part of the West Bank (see Figure 1 and 2). It is one of the 33 catchments throughout the West Bank, with an area of approximately 320 km^2 (Shadeed *et al.* 2017), which constitutes about 6% of the West Bank area (Abedel-Kareem 2005). The Faria catchment is characterized as agricultural, where its land is agricultural land, as this is due to the quality of arable soil as well as the availability of water, where many groundwater wells are observed in the catchment, which increases agricultural activity in the area. The Faria catchment is characterized by its Mediterranean semi-arid climate, which has a rainy and relatively cold winter and a hot and dry summer. The rainfall period extends for 6 months from October to April of the year, and most of the rainfall falls in this period; for the remaining 6 months, it is a relatively dry summer. The annual temperature in the catchment ranges from about 18 °C at the northwestern side to about 24 °C at the south-eastern side at the outlet near the Jordan River (Abu Hijleh 2014). The amount of rainfall in the catchment varies considerably, as this is due to the large disparity in the topography, which significantly affects the climate. The amount of rainfall in the Faria catchment ranges from about 640 mm at the top of the catchment to about 150 mm at the bottom (the outlet) near the Jordan River (Haji 2017). Quantities vary as we go from west to east, as well as north to south.

Elevations of the Faria catchment are characterized by high variability of elevations throughout a small area, ranging from about 901 m amsl in the Nablus Mountains in the north to about 350 m bmsl at the outlet of the catchment in the Jordan River region. The Faria catchment is monitored by six rainfall stations: Nablus, Al-Faria, Talluza, Tubas, Tammun, and Beit Dajan. Nablus serves as the primary weather station, providing comprehensive weather data. The other stations are basic rain gauges measuring daily rainfall (Shadeed *et al.* 2014).

Water sources in the Faria catchment are classified as either surface water or groundwater, and the area is classified as being mainly within the Eastern Ground Basin. There are about 71 groundwater wells in the region, most of which are

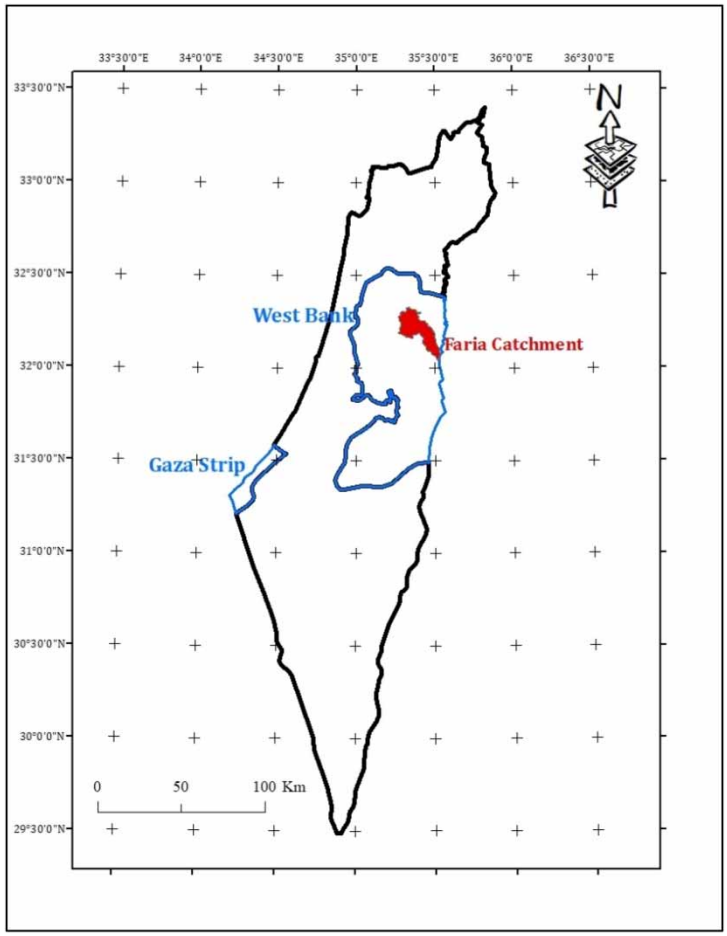

Figure 1 | Location of the Faria catchment.

classified for agricultural purposes, where the depth ranges from 10 to 190 m, as the total use of groundwater wells ranges from 4.4 to 11.5 MCM annually. Another source of water is springs, where they are the only natural outlet for drainage of groundwater in the catchment. There are 11 springs in the upper and middle parts of the catchment. The values of the discharge for these springs range from about 1.4 to 40 MCM (Shadeed 2008). In addition, surface water flows from north to southeast within the catchment, comprising runoff from eastern Nablus, Tubas, and Tammun sub-areas, discharges from the Faria refugee camp at the catchment headwaters, and spring-fed contributions that sustain baseflow, preventing summer drying of the valley. This system also receives untreated sewage inputs from eastern Nablus and the Al-Faria refugee camp (Sulaiman 2017).

2.2. Data

The accuracy and robustness of any hydrological simulation rest on the quality and representativeness of its input datasets. For climate projections in this study, we leverage long-term, bias-corrected WorldClim (1 km) and CRUTS4.05 archives to capture trends in rainfall, temperature, humidity, wind speed, and solar radiation. In the river-flow modeling phase (ArcSWAT), daily rainfall records from six local gauge stations (1990–2021) are integrated with co-located meteorological variables, temperature, humidity, wind speed, and solar radiation sourced from NASA-POWER (0.5° × 0.5° grid). High-resolution topography is provided by a 25 m × 25 m digital elevation model (DEM), while land use and soil characteristics are obtained from the national Geomolg repository and the FAO Global Soil Dataset, respectively. Finally, observed streamflow data from Parshall flumes at the Badan sub-catchment (2004–2007) (1/11/2004 to 9/3/2005, 1/10/2005 to 16/3/2006, and 15/11/2006 to 28/3/2007) underpin model calibration and validation. Full metadata for all input datasets are summarized in Table 1.

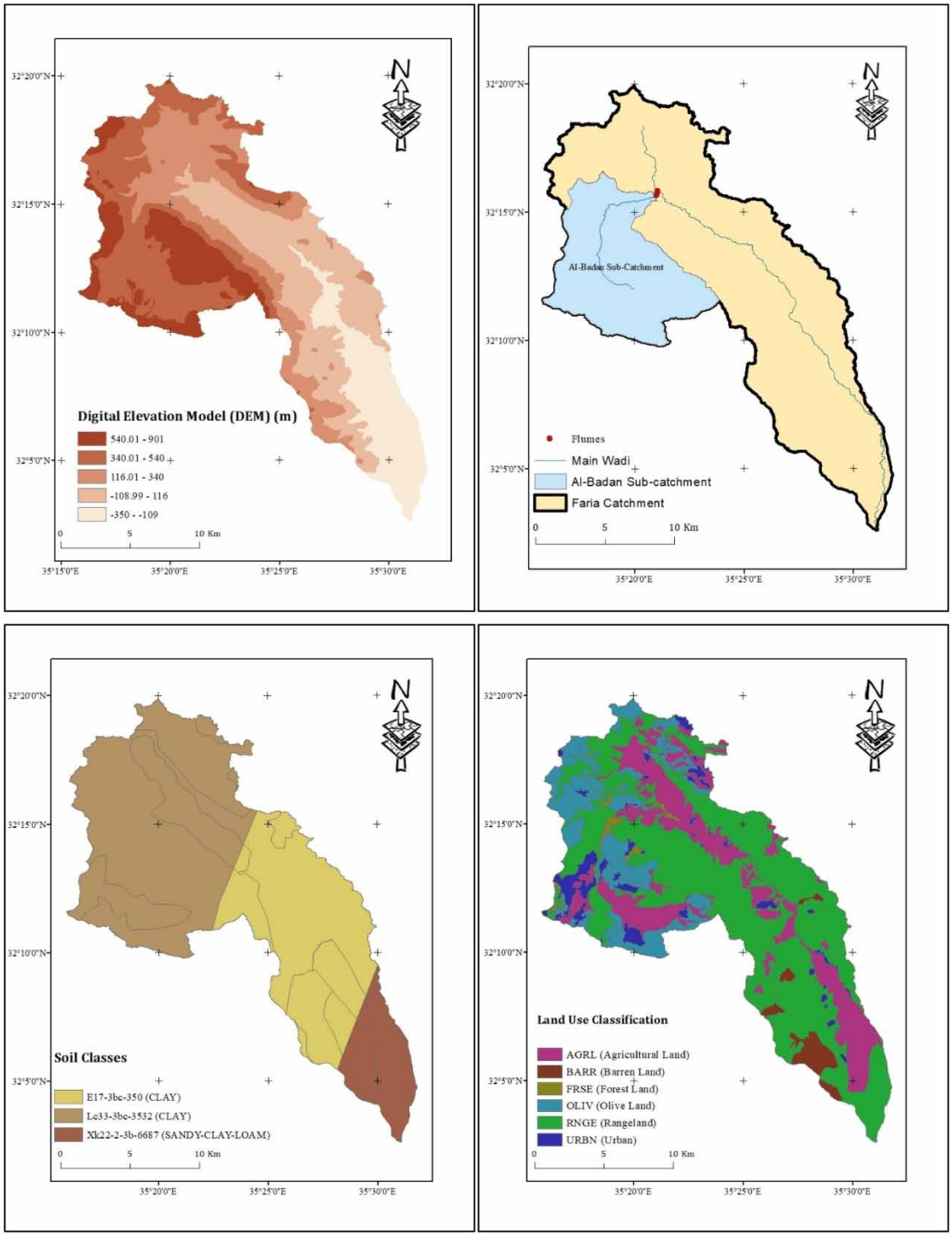

Figure 2 | DEM, land use map for the SWAT model, SWAT soil classifications for the Faria catchment, and the Badan sub-catchment (Geographic Coordinate System: GCS_WGS_1984).

2.3. Rainfall stations

The number of stations used to represent rainfall is important for the accuracy of work in the calculation of the rainfall for a given area, in order to be well represented and spread over the entire area, where the optimal number of stations required is

Table 1 | Summary of the key attributes of each dataset

Data	Source	Period	Resolution
Rainfall	Palestinian Meteorological Department	1990–2021	Point gauges
Temperature, relative humidity, wind speed, solar radiation	NASA-POWER	1990–2021	0.5° × 0.5°
Digital elevation model (DEM)	Geomolg (Palestinian MoLG & GIZ)	–	25 m × 25 m
Land use	Geomolg	–	30 m × 30 m
Soil properties	FAO Global Soil Dataset	–	~1 km × 1 km
GCM climate projections (23 models)	SimClim AR6	2060, 2100	Varies by model
Streamflow (Badan sub-catchment)	Parshall flumes	2004–2007	Daily

calculated by Equation (1) (Shadeed 2008):

$$N = \left(\frac{C_v}{E_p}\right)^2 \tag{1}$$

where N is the optimal number of stations; C_v is the coefficient of variation of the rainfall from the existing stations in percentage; and E_p is the allowable percentage of error in the estimation of the aerial mean rainfall.

To calculate the coefficient of variation (C_v), the following steps were applied:

Six current stations' rainfall data were used to generate the previous statistical parameters, the allowable percentage of error was assumed to be 11% (Shadeed 2008); the optimal number of stations $N = 15$, then the additional station $= N - n = 9$. The additional nine stations were added so that they are well spatially distributed throughout the catchment and are representative, also the mean annual rainfall for the stations were calculated using Equation (2) (see Figure 3).

The amounts of rainfall in the Faria catchment are affected by the elevations, as the amount of rainfall increases with the increase in elevation. A spatial relationship was developed to estimate the average annual rainfall for the stations by Abedel-Kareem (2005), where multiple linear regression was used for five stations within the catchment (Nablus, Talluza, Beit Dajan, Tubas, and Tammun), which depends on the spatial coordinates (Palestinian coordinates) of the station as well as the elevation, as Equation (2):

$$R = 8,285 - 39.41X - 2.46Y - 0.34Z \tag{2}$$

where R is the annual average rainfall of the station (mm), X and Y are the geographic Palestinian coordinates (km), and Z is the elevation (m).

The sixth station (Al-Faria station) was used to verify the relationship (Haji 2017).

Filling the missing rainfall data is essential to complete all the necessary rainfall data and thus the success of the model. The estimate for each day of missing reading at a particular station is based on the data observed on that day for the Faria catchment stations and on the average for each station. There is no day for which there are no known values.

2.4. General circulation models

Future climate predictions based on general circulation models (GCMs) form a solid scientific basis for assessing the impacts of climate change. In the Faria catchment, where this study is being conducted for the first time at the regional level, using an individual GCM is an unreliable methodology due to the absence of robust criteria for preferring one model over another. Accordingly, we adopted a multi-model ensemble approach to integrate the outputs of 23 GCMs via the SimClim AR6 platform, applying the statistical median rather than the arithmetic mean to process the data. To further enhance reliability, SimClim automatically performs spatial bias correction for the baseline period by statistically combining high-resolution WorldClim 2.1 data with CRUTS4.05 observations, generating an optimized and homogeneous reference dataset. This combined approach, the ensemble median and the bias correction, ensures that the impact of outliers and inherent model biases is minimized (Urich *et al.* 2014), providing a more balanced and representative projection of future climate during the 2060 and

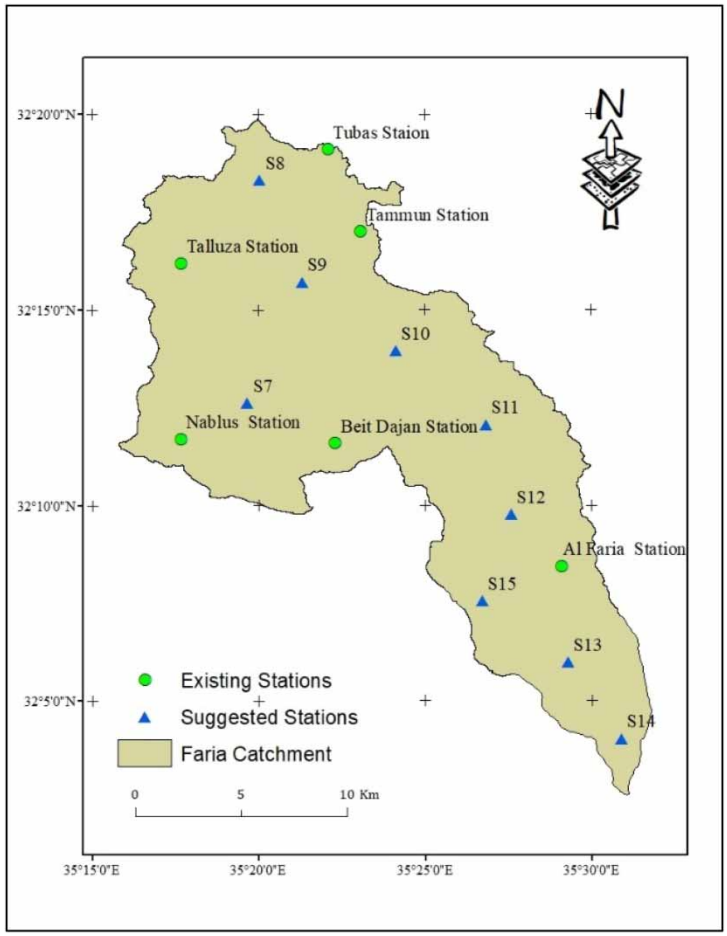

Figure 3 | The distribution of the existing and the suggested stations in the Faria catchment.

2100 periods. The 23 identifiable models within SimClim AR6 provide all necessary meteorological variables (rainfall, temperature, relative humidity, wind speed, and solar radiation) (Saade *et al.* 2021) (see Table 2).

2.5. Shared Socioeconomic Pathways

For the CMIP6 where it relied on SSPs, where these scenarios are considered to be more comprehensive because they include social and economic factors as well as greenhouse gas emissions (Riahi *et al.* 2017), where scenarios range between SSP1-1.9, SSP1-2.6, SSP2-4.5, SSP3-7.0, and SSP5-8.5, where SSP2-4.5 represents a scenario that is expected to continue with current trends in terms of social and economic growth, while SSP5-8.5 represents a scenario of increase in rapid innovation and technological progress but with intense reliance on fossil fuels, thus increasing greenhouse gas emissions (Tebaldi *et al.* 2020). This study will include two scenarios, SSP2-4.5 and SSP5-8.5, which are included in the SimClim AR6 software for several GCMs, where the medium scenario was chosen as the most likely for the current situation, while the high scenario was selected to understand the potential prospects for the most severe future situation and for two periods of time (2060 and 2100).

2.6. Model setup

Hydrological modeling was performed with SWAT2012 via ArcSWAT, where a drainage-area threshold of 320 km^2 was applied during watershed delineation to generate 33 sub-basins (Figure 4).

Semi-arid catchments such as the Faria catchment are typically characterized by high rainfall variability, intense but short wet seasons, and extended dry periods. These conditions often lead to rapid SRO due to low soil infiltration capacity, minimal baseflow contribution in dry months, and highly seasonal groundwater recharge. These hydrological characteristics

Table 2 | GCMs selected in the SimClim AR6

Institution	Model name (in SimClim)	Horizontal resolution (lat. × lon.)
Australian Research Council Centre of Excellence for Climate System Science, Australia	ACCESS-CM2	1.25° × 1.875°
	ACCESS-ESM1-5	1.25° × 1.875°
Canadian Centre for Climate Modelling and Analysis, Canada	CanESM5	2.8° × 2.8°
	CanESM5-CanOE	2.8° × 2.8°
Chinese Academy of Sciences, China	CAS-ESM2-0	1.0° × 1.0°
Euro-Mediterranean Center on Climate Change, Italy	CMCC-ESM2	1.25° × 0.9375°
National Center for Meteorological Research, France	CNRM-CM6-1	1.4° × 1.4°
	CNRM-CM6-1-HR	1.4° × 1.4°
	CNRM-ESM2-1	1.4° × 1.4°
Swedish Meteorological and Hydrological Institute, Sweden	EC-Earth3-AerChem	0.7° × 0.7°
	EC-Earth3-Veg-LR	0.7° × 0.7°
National Aeronautics and Space Administration, USA	GISS-E2-1-G	2° × 2.5°
The UK Meteorological Office, UK	HadGEM3-GC31-LL	1.25° × 1.875°
	HadGEM3-GC31-MM	1.25° × 1.875°
	UKESM1-0-LL	1.25° × 1.875°
Russian Academy of Science, Russia	INM-CM4-8	1.5° × 2°
	INM-CM5-0	1.5° × 2°
Institute Pierre Simon Laplace, France	IPSL-CM6A-LR	1.26° × 2.5°
Japan Agency for Marine-Earth Science and Technology, Japan	MIROC6	1.4° × 1.4°
	MIROC-ES2L	2.8° × 2.8°
Max Planck Institute for Meteorology, Germany	MPI-ESM1-2-HR	0.9375° × 0.9375°
	MPI-ESM1-2-LR	1.875° × 1.875°
Meteorological Research Institute, Japan	MRI-ESM2-0	1.125° × 1.125°

underscore the importance of using a physically based, distributed model like SWAT, which can represent these spatial and temporal dynamics with suitable resolution and accuracy.

Hydrological response units (HRUs), defined as areas sharing homogeneous land use, soil type, and slope characteristics, were initially generated through the intersection of sub-basin, land use, soil, and slope layers, yielding 597 HRUs. These HRUs were subsequently generalized using dominance thresholds of 10% for land use, 20% for soil type, and 10% for slope. Water balance parameters were computed utilizing the curve number method for runoff estimation (Neitsch *et al.* 2002) and the Penman–Monteith method for potential evapotranspiration (PET).

Due to the limited length of observed streamflow data (2004–2007), the SWAT model was run without a designated warm-up period, which is acknowledged as a limitation. Nonetheless, given the 32-year simulation span, this decision is supported by SWAT Manual guidelines (p. 61) (Neitsch *et al.* 2002) stating that warm-up is optional for simulations exceeding 30 years, and by findings from 2018 (Kim *et al.* 2018), which indicate that even under worst-case conditions, warm-up durations are $\leq$6 months (<2% of our simulation) with negligible impact on long-term statistical metrics (Kim *et al.* 2018).

The SWAT evaluation process is critical to ensure its performance and thus to ensure proper outputs, using two key parameters for evaluating its performance that are present within the Sequential Uncertainty Fitting Algorithm (SUFI-2), which are the coefficient of determination (R^2) and the Nash–Sutcliffe efficiency (NSE) (Legesse Gebre 2015). These parameters are the most common and comprehensive in assessing the SWAT model for calibration and verification phases (see Table 3). R^2 is a measurement of the compatibility of the model's results and measured values. Equation (3) shows the R^2 formula:

$$R^2 = \frac{\left[\sum_{i=1}^{n} (Q_{\text{obs}}(i) - \overline{Q_{\text{obs}}})(Q_{\text{sim}}(i) - \overline{Q_{\text{sim}}})\right]^2}{\sum_{i=1}^{n} (Q_{\text{obs}}(i) - \overline{Q_{\text{obs}}})^2 \sum_{i=1}^{n} (Q_{\text{sim}}(i) - \overline{Q_{\text{sim}}})^2} \quad (3)$$

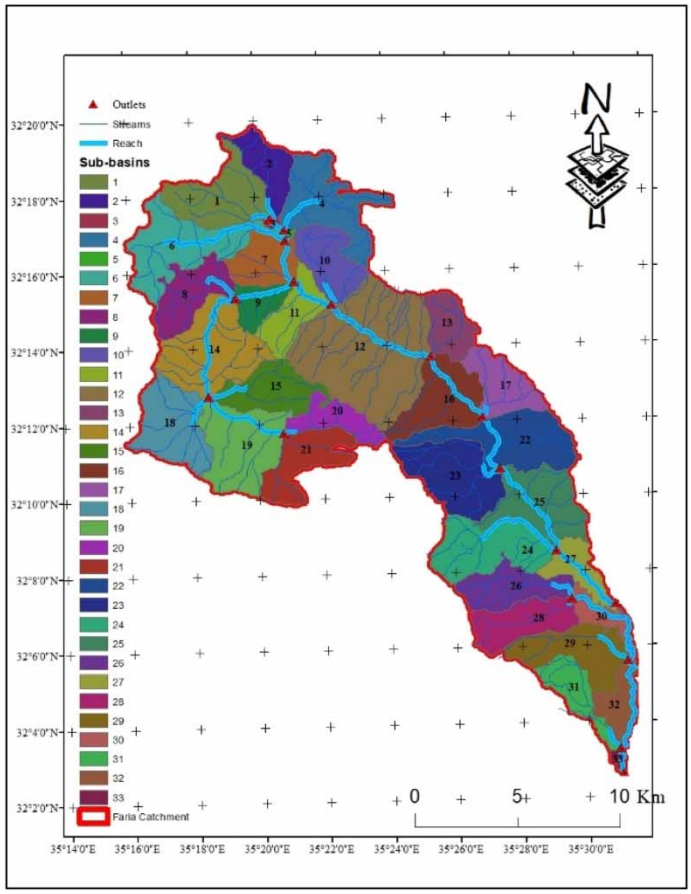

Figure 4 | Sub-basins, outlets, reaches, and the streams of the Faria catchment.

Table 3 | The model's performance ratings according to the parameters in its evaluation (Pérez-Sánchez *et al.* 2019)

Classification	NSE	R^2
Very Good	$0.75 < \text{NSE} \leq 1.00$	$0.85 < R^2 \leq 1.00$
Good	$0.65 < \text{NSE} \leq 0.75$	$0.75 < R^2 \leq 0.85$
Satisfactory	$0.50 < \text{NSE} \leq 0.65$	$0.60 < R^2 \leq 0.75$
Unsatisfactory	$\text{NSE} \leq 0.50$	$R^2 \leq 0.60$

where Q_{obs} indicates the observed flow values, Q_{sim} indicates the simulated values, $\overline{Q_{obs}}$ is the average observed flow, and $\overline{Q_{sim}}$ is the average of the simulated flow. R^2 values range from 0 to 1, so that the higher the value, the better the model's representation, and indicates a perfect correlation between the results and the observed values.

The NSE refers to goodness's assessment of the model from the convergence of simulation with observed values, and its values range from $-\infty$ to 1, whereas the values ≤ 0 indicates that the model is not reliable and when the values close to 1, this indicates the convergence of the simulated and observed values, where Equation (4) shows the NSE formula (Mendoza *et al.* 2021):

$$\text{NSE} = 1 - \frac{\sum_{i=1}^{n} \left(Q_{obs}\ (i) - Q_{sim}\ (i)\right)^2}{\sum_{i=1}^{n} \left(Q_{obs}\ (i) - \overline{Q_{obs}}\right)^2} \tag{4}$$

3. RESULTS

3.1. Simclim AR6 results and analysis

SimClim AR6 projections indicate substantial alterations in meteorological variables across the Faria catchment under both emission scenarios, as shown in Table 4. By 2060 under SSP2-4.5, annual rainfall declines by 5.77–6.82%, intensifying to 17.64–20.88% by 2100 under SSP5-8.5 (see Figure 5). Concurrently, minimum temperatures rise by 2.26–2.32 °C (SSP2-4.5, 2060) and 6.90–7.11 °C (SSP5-8.5, 2100), while maximum temperatures increase by 2.36–2.47 °C by 2060 under SSP2-4.5 and

Table 4 | Projected changes in meteorological variables

Meteorological variable	SSP2-4.5 (2060)	SSP2-4.5 (2100)	SSP5-8.5 (2060)	SSP5-8.5 (2100)
Rainfall	–5.77 to –6.82%	–8.69 to –10.15%	–8.43 to –9.84%	–17.64 to –20.88%
Minimum temperature	+2.26 to +2.32 °C	+3.36 to +3.47 °C	+3.26 to +3.36 °C	+6.90 to +7.11 °C
Maximum temperature	+2.36 to +2.47 °C	+3.52 to +3.69 °C	+3.41 to +3.57 °C	+7.22 to +7.57 °C
Relative humidity	–0.96 to –1.40%	–1.44 to –2.09%	–1.39 to –2.02%	–3.55 to –4.28%
Solar radiation	+1.16 to +1.30%	+1.76 to +1.94%	+1.68 to +1.88%	+3.55 to +3.98%
Wind speed	–0.22 to +0.36%	–0.33 to +0.54%	–0.32 to +0.52%	–0.68 to +1.09%

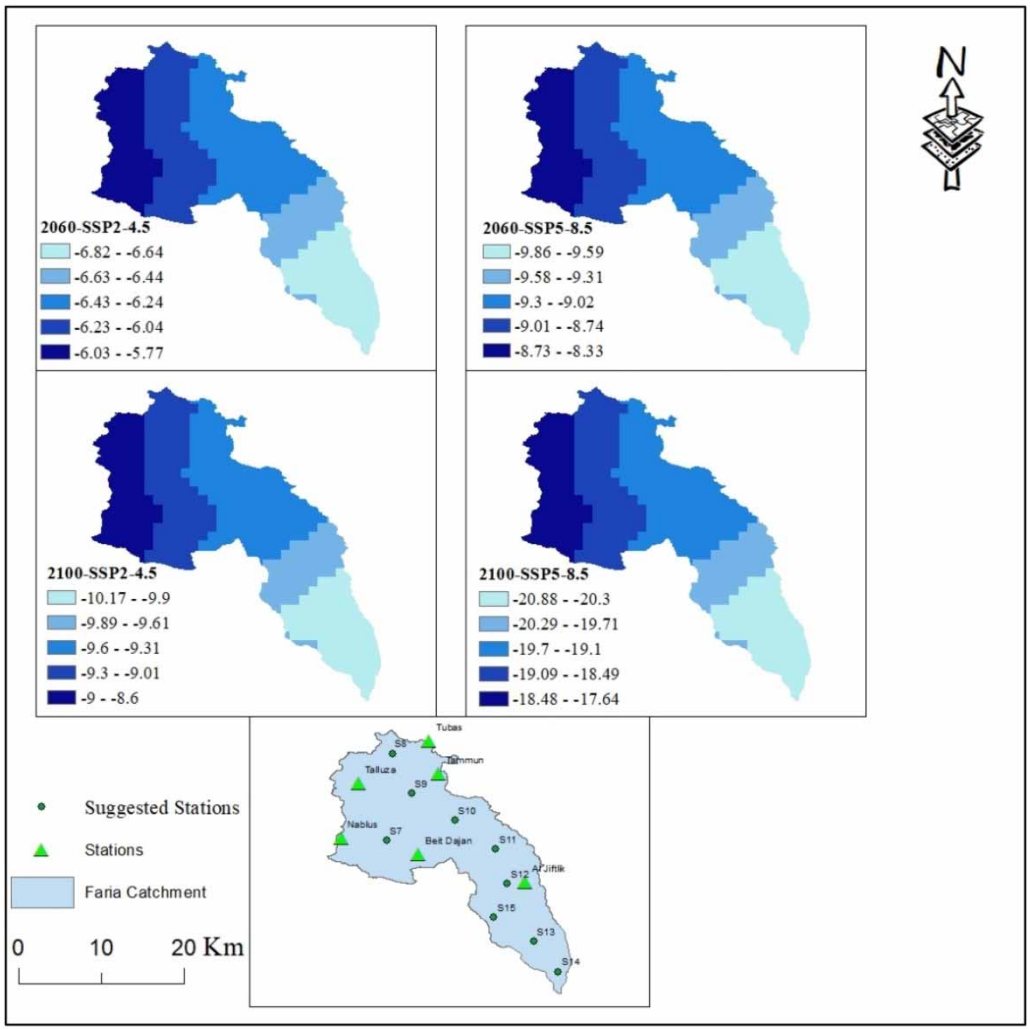

Figure 5 | Spatial rainfall changes in the Faria catchment.

7.22–7.57 °C by 2100 under SSP5-8.5. Relative humidity decreases by up to 4.28% by 2100 under SSP5-8.5, and solar radiation rises by 3.55–3.98% under the same scenario. Wind speed exhibits minimal spatial variability. These shifts collectively signal a transition toward hotter, drier conditions.

3.2. Hydrological model performance

Parameter optimization and uncertainty analysis were conducted in SWAT-CUP using the SUFI-2 algorithm, which systematically samples parameter ranges, quantifies output uncertainty through prediction-uncertainty bands, and ranks parameter sensitivity, thus ensuring that both calibration performance and model reliability are rigorously assessed (Abbaspour 2015). SUFI-2 efficiently handles multiple parameters and allows simultaneous calibration across sub-basin outlets, improving the model's overall performance. Sensitivity analysis was based on daily streamflow data from the Badan sub-catchment (outlet No. 9). The process started with 25 flow-related parameters and, after several iterations, was reduced to 15 of the most influential ones. Each iteration included at least 50 simulations, aiming to optimize statistical indicators like the coefficient of determination (R^2) and NSE, as recommended for watershed model evaluation (Moriasi *et al.* 2007). This calibration strategy has been effectively applied in similar catchments under limited data conditions and in semi-arid environments, where SUFI-2 has demonstrated reliability and adaptability for managing hydrological uncertainty (Jahanshahi *et al.* 2017).

Table 5 presents the final set of parameters used at outlet No. 9. Parameters labeled with 'v_' represent absolute values directly adjusted during calibration, while those marked 'r_' indicate relative changes from baseline values. This distinction, aligned with SWAT-CUP conventions, facilitates the interpretation of parameter behavior and their role in model optimization.

The values obtained at the calibration stage using observed data for the period (2004–2006), $R^2 = 0.67$ and NSE = 0.64, while the values for the validation phase using data for the period (2006–2007) were $R^2 = 0.73$ and NSE = 0.52. Figure 6 represents the comparison between the observed and simulated data values for the calibration and the validation phases.

A slight decrease in NSE = 0.52 is observed during validation compared with calibration, despite a higher coefficient of determination ($R^2 = 0.73$). This is attributed to NSE's high sensitivity to errors in peak flow, low flow, and timing offset simulations, while R^2 reflects the strength of the overall linear trend. Aggregate performance remains satisfactory in the context of a semi-arid catchment.

A focused sensitivity analysis identified the most influential parameters driving model outputs (see Table 6). Among these, the CN2 (curve number) parameter had the highest sensitivity, highlighting its key role in regulating SRO generation. It was

Table 5 | Fitted values for the selected parameters

Parameter	Description	Unit	Fitted value	Absolute range	
				Min	Max
V__CN2.mgt	SCS runoff curve number	–	56	35	98
R__SOL_BD().sol	Moist bulk density	g/cm^3	0.396	−0.1	1
R__ALPHA_BF.gw	Baseflow alpha factor	days	0.951	0	1
R__HRU_SLP.hru	Average slope steepness	%	0.234	0	1
R__SOL_K(..).sol	Saturated hydraulic conductivity	mm/h^1	−0.146	−0.2	0.1
V__EPCO.bsn	Plant uptake compensation factor	–	0.7025	0	1
V__ESCO.bsn	Soil evaporation compensation factor	–	0.9382	0	1
R__SOL_AWC(..).sol	Available water capacity of the soil layer	mm/mm^1	0.085	−0.1	0.1
V__GWQMN.gw	Threshold depth of water in the shallow aquifer required for return flow to occur	mm	3,182.5	0	4,000
V__GW_DELAY.gw	Groundwater delay	days	204.796	0	450
R__RCHRG_DP.gw	Deep aquifer percolation fraction	–	0.0741	0	0.1
V__REVAPMN.gw	Threshold depth of water in the shallow aquifer for 'revap' to occur	mm	237.5	0	500
R__CH_S2.rte	Average slope of the main channel	(m/m^1) (%)	4.453	−0.001	10
R__OV_N.hru	Manning's '*n*' value for overland flow	–	27.4	0.01	30
V__SLSUBBSN.hru	Average slope length	m	62.5	0	150

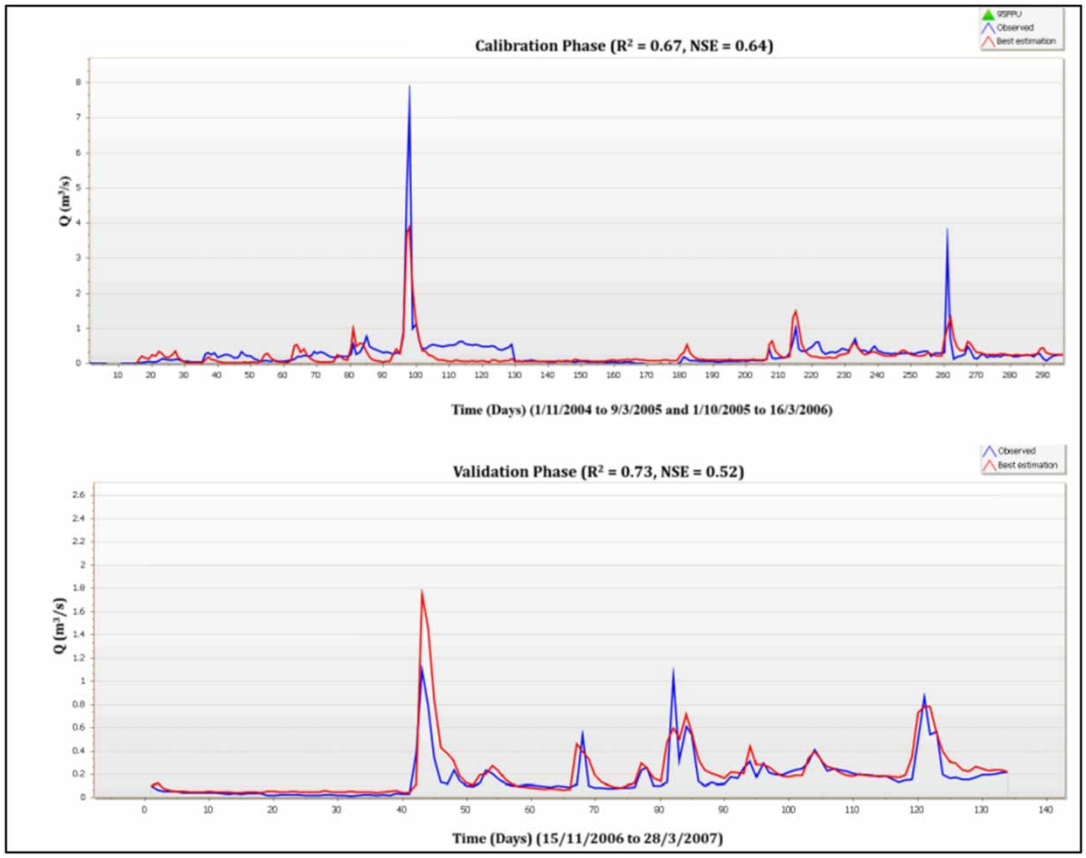

Figure 6 | Comparison between observed and simulated values for calibration and validation stages. *Note*: The difference between R^2 and NSE during validation reflects NSE's sensitivity to errors in the magnitude and timing of extreme events versus R^2's focus on overall trend accuracy.

Table 6 | Sensitivity analysis for SWAT-CUP parameters

Rank	Parameter name	*t*-Stat	*P*-value
1	V__CN2.mgt	−7.18	0
2	R__RCHRG_DP.gw	4.64	0.01
3	R__CH_S2.rte	−3.97	0.02
4	R__HRU_SLP.hru	−2.56	0.06
5	R__SOL_BD(..).sol	2.21	0.09
6	R__SLSUBBSN.hru	−1.84	0.14
7	V__GW_DELAY.gw	−1.39	0.24
8	R__ALPHA_BF.gw	−1	0.37
9	V__REVAPMN.gw	−0.95	0.39
10	V__ESCO.bsn	−0.94	0.4
11	V__EPCO.bsn	0.8	0.47
12	R__SOL_K(..).sol	0.8	0.47
13	R__SOL_AWC(..).sol	0.42	0.69
14	V__GWQMN.gw	0.3	0.78
15	R__OV_N.hru	−0.28	0.79

followed by RCHRG_DP (deep aquifer percolation) and CH_S2 (channel slope), which significantly influence infiltration and channel flow velocity. Other moderately sensitive parameters included HRU_SLP and SOL_BD, reflecting the role of topographic slope and soil properties in controlling runoff response. These findings are consistent with hydrological behavior in semi-arid systems, where small changes in land surface and soil conditions can lead to pronounced shifts in catchment hydrodynamics.

3.3. Water budget components

The water budget elements in the Faria catchment are influenced both spatially and temporally by climate change, which significantly alters rainfall patterns and other meteorological variables. These changes affect key hydrological components, including SRO, ET, WY, and groundwater recharge, at both the sub-basin scale and monthly level during the future periods of 2060 and 2100 under the SSP2-4.5 and SSP5-8.5 scenarios.

In SWAT, WY is defined as the total water volume that exits a HRU and reaches the main channel. It consists of SRO, lateral flow, and baseflow. The baseflow component is estimated using a simplified linear reservoir approach, which may not fully capture delayed groundwater contributions from deeper aquifer layers. As a result, groundwater-fed streamflow, especially during dry periods, may be underestimated.

SRO in the catchment is higher in the upper parts, while it is significantly lower in the lower parts, as this is due to the rise in annual rainfall in the upper parts and conversely in the lower parts. The results indicated a significant decrease in the SRO under the two emission scenarios. The highest amount of SRO is about 175.72 mm in sub-basin 18, where it decreased by 11.25 and 16.11% for the 2060, under the SSP2-4.5 and SSP5-8.5 scenarios, respectively, while decreasing by 16.61 and 33.03% for the 2100 period under the SSP2-4.5 and SSP5-8.5 scenarios, respectively. Figure 7 shows the spatial distribution of SRO in the Faria catchment under the scenarios of climate change for the two time periods.

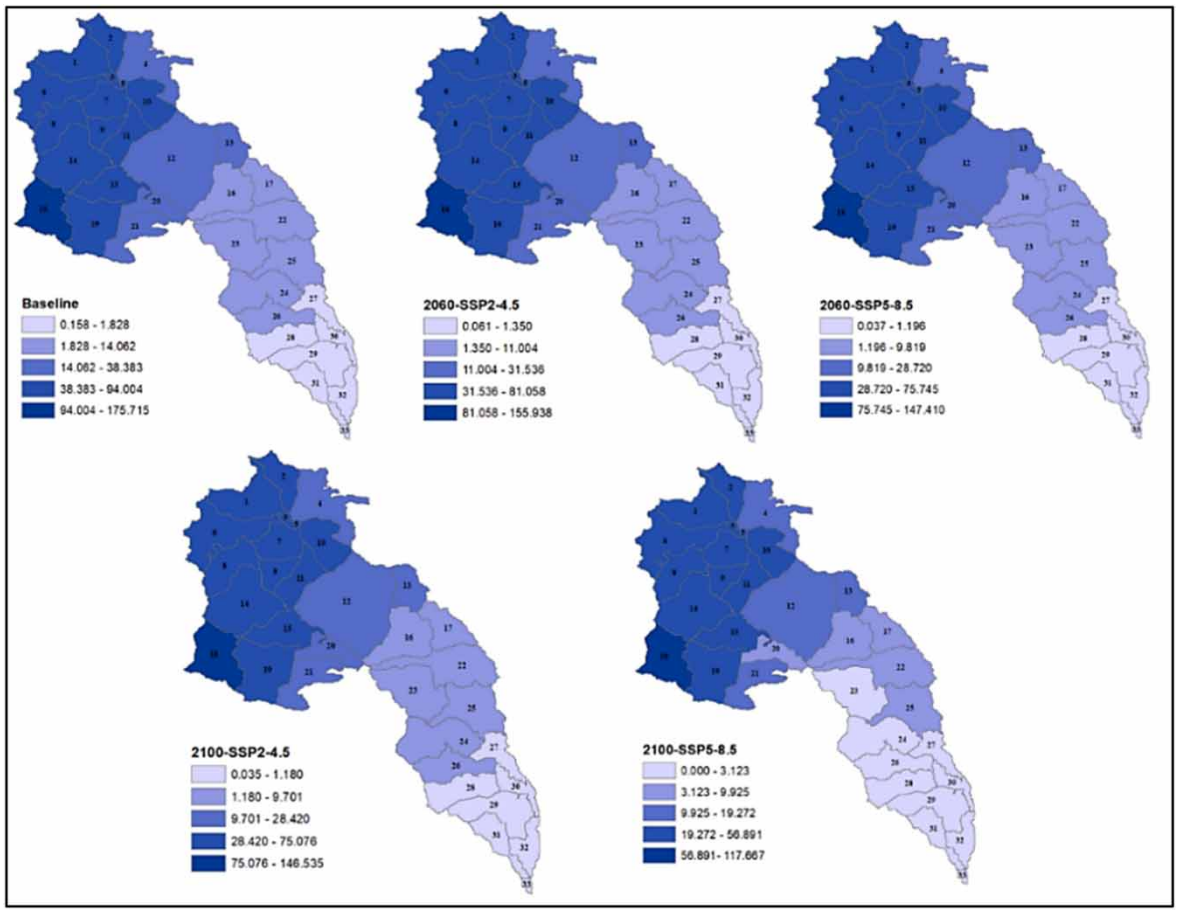

Figure 7 | Spatial distribution of the surface runoff in the Faria catchment under SSP2-4.5 and SSP5-8.5 for 2060 and 2100.

ET outcomes showed an increase over various sub-basins, where the lower value based on baseline results in sub-basin 6 was about 83.008 mm, where the value had changed by 3.53, 0.225, 5.08, and 9.79% under the scenarios of SSP2-4.5 and SSP5-8.5 for 2060 and 2100, respectively, indicating a rise in ET values overall. While the highest values reached about 143.68 mm in sub-basin 3 in an SSP5-8.5 scenario in the 2100 period, where the increase was 2.3% over the baseline. Figure 8 refers to the spatial distribution of ET values in the basin under the SSP2-4.5 and SSP5-8.5 scenarios for the two periods.

Climate change negatively impacted WY with a significant decrease in all scenarios, with the WY reflecting the amount of water leaving the HRUs and entering the mainstream during the time step, as lower rainfall rates and higher minimum and maximum temperatures, as well as changes in the relative humidity, solar radiation, and wind speed, have demonstrated their impact on WY. WY values are higher in the above parts in the catchment, due to high rainfall rates, with the highest values being about 445.19 mm in sub-basin 18, while the value under the two emissions scenarios changed by −8.07, −12.77, −13.17, and −29.7% for 2060 and 2100, respectively (see Figure 9).

The results indicated a decrease in the groundwater recharge values, due to low rainfall rates and high ET rates, where the highest value in the catchment was in sub-basin 8 where the value is 259.972 mm, where it changed by −9.28 and −11.08% for the 2060 period under the SSP2-4.5 and SSP5-8.5 scenarios, respectively, while it changed by −13.95 and −29.07% for the 2100 period under the SSP2-4.5 and SSP5-8.5 scenarios, respectively (see Figure 10).

Monthly analyses reveal critical shifts in hydrological behavior (Figure 11). ET peaks intensified during summer months due to temperature amplification. SRO and groundwater recharge diminished during winter (January–March), reducing dry-season baseflow. WY declines were most pronounced in spring (April–June), coinciding with peak agricultural water demand. These temporal changes exacerbate water stress during critical growth periods.

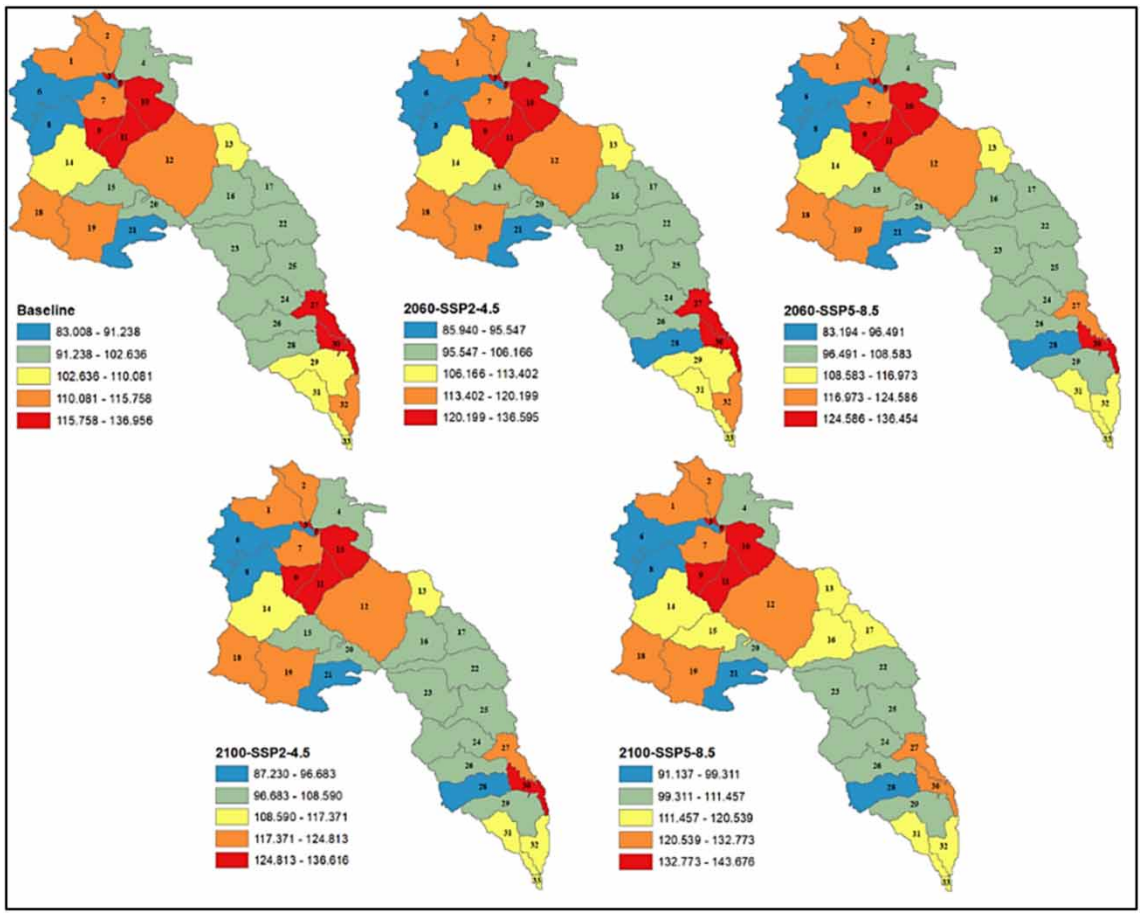

Figure 8 | Spatial distribution of the evapotranspiration in the Faria catchment under SSP2-4.5 and SSP5-8.5 for 2060 and 2100.

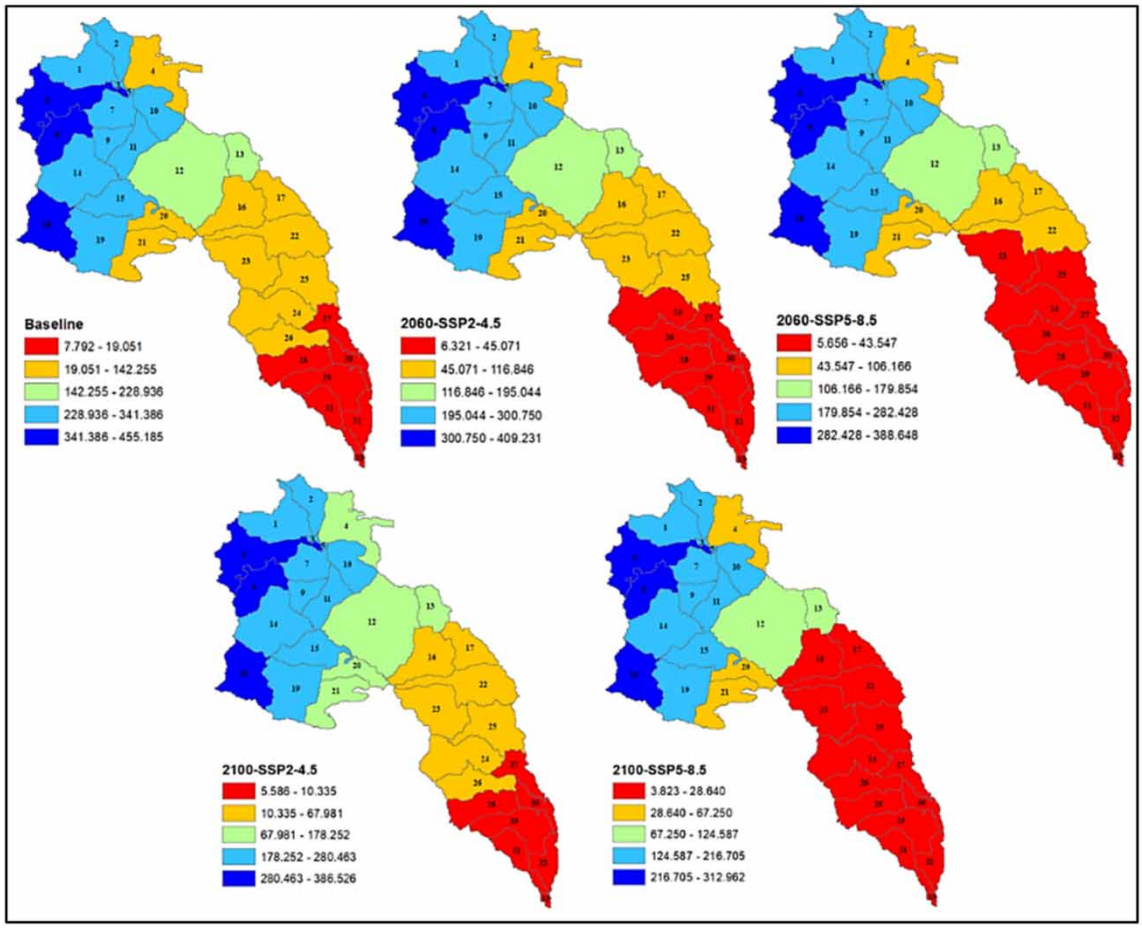

Figure 9 | Spatial distribution of the water yield in the Faria catchment under SSP2-4.5 and SSP5-8.5 for 2060 and 2100.

Although the present analysis emphasizes long-term mean changes in hydrological components, the projected climatic shifts under SSP5-8.5, particularly increased temperature and decreased relative humidity, also suggest an elevated likelihood of hydrological extremes. These include prolonged dry periods and more intense short-duration rainfall events, which may increase both drought frequency and flash flood potential. While this study did not explicitly simulate extreme events, the findings strongly point to the necessity of incorporating extreme-event analysis in future hydrological assessments for effective risk mitigation and adaptive planning in the Faria catchment.

4. DISCUSSION

The assessment of climate change impacts on water budget components in the Faria catchment was conducted using the SWAT2012 model. Spatial bias in metrological data was corrected using SimClim AR6, WorldClim 2.1, and CRUTS4.05, incorporating five daily meteorological variables (rainfall, minimum and maximum temperatures, relative humidity, solar radiation, and wind speed) over the baseline period (1990–2021).

The projected reduction in total WY signals a fundamental hydrological shift driven by multiple stressors, including reduced rainfall, increased temperatures, intensified ET, and increasing solar radiation. Seasonal analysis of monthly hydrological dynamics reveals a critical temporal mismatch between water supply and agricultural demand. SRO and groundwater recharge are concentrated in the rainy winter season (December–March), whereas both decline sharply from spring onward. Notably, actual ET does not peak in the midsummer months (July–August), despite extremely high temperatures and radiation levels. This is explained by the fact that, while PET is at its highest during these months, actual ET is constrained by severely limited soil moisture and vegetation stress. In contrast, spring months (April–June) show moderate ET levels due to residual

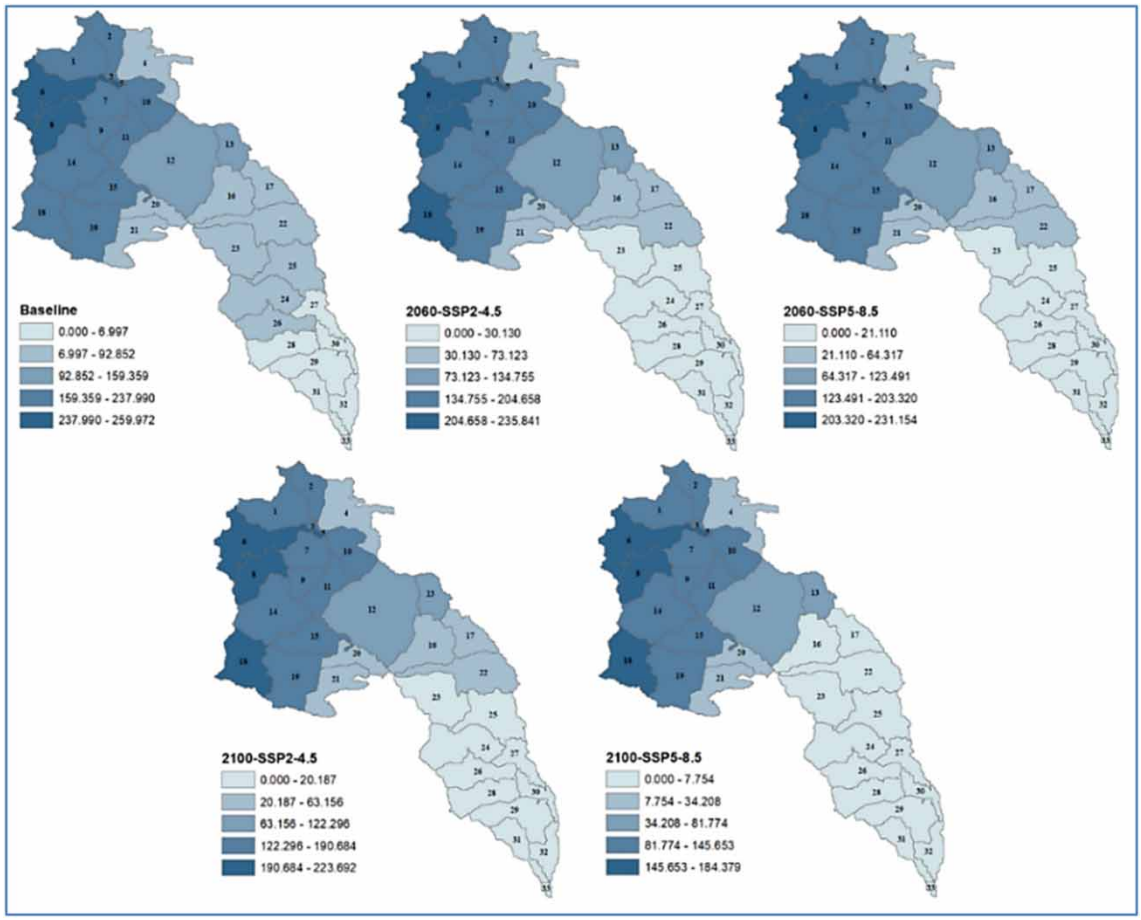

Figure 10 | Spatial distribution of the groundwater recharge in the Faria catchment under SSP2-4.5 and SSP5-8.5 for 2060 and 2100.

soil moisture from winter rainfall, coinciding with peak crop water requirements. This seasonal decoupling, where PET is highest when available water is lowest, intensifies agricultural vulnerability under future climate scenarios. These dynamics highlight the need for adaptive water management strategies, including seasonal water storage, managed aquifer recharge, and optimized irrigation scheduling.

These trends pose significant risks to rain-fed agriculture in one of Palestine's most critical food-producing regions. Simulations identified key mechanisms behind this shift, diminished rainfall intensity limiting infiltration and SRO; elevated atmospheric demand increasing ET and reducing groundwater recharge; and compressed wet seasons failing to adequately replenish aquifers.

While air temperature is expected to rise by more than 7 °C under the SSP5-8.5 scenario by 2100, the corresponding increase in ET remains relatively modest (3–10%). This discrepancy is further explained by limited soil moisture availability, which constrains actual ET despite elevated PET. Additionally, vegetation stress and shortened growing seasons under high-emission scenarios may suppress plant transpiration and further limit ET increases.

The projected decline in groundwater recharge, especially under SSP5-8.5, indicates mounting pressure on subsurface water reserves. This reduction is likely to decrease baseflow contributions during the dry season and threaten aquifer sustainability. In the Faria catchment, where 71 agricultural wells are active, declining recharge may undermine irrigation reliability and domestic supply, intensifying water insecurity during prolonged droughts.

Model calibration and validation were conducted using observed streamflow records, with a calibration phase (2004–2006; $R^2 = 0.67$, NSE = 0.64) and a validation phase (2006–2007; $R^2 = 0.73$, NSE = 0.52). Sensitivity analysis identified CN2 (curve number) as the most influential parameter affecting model outputs.

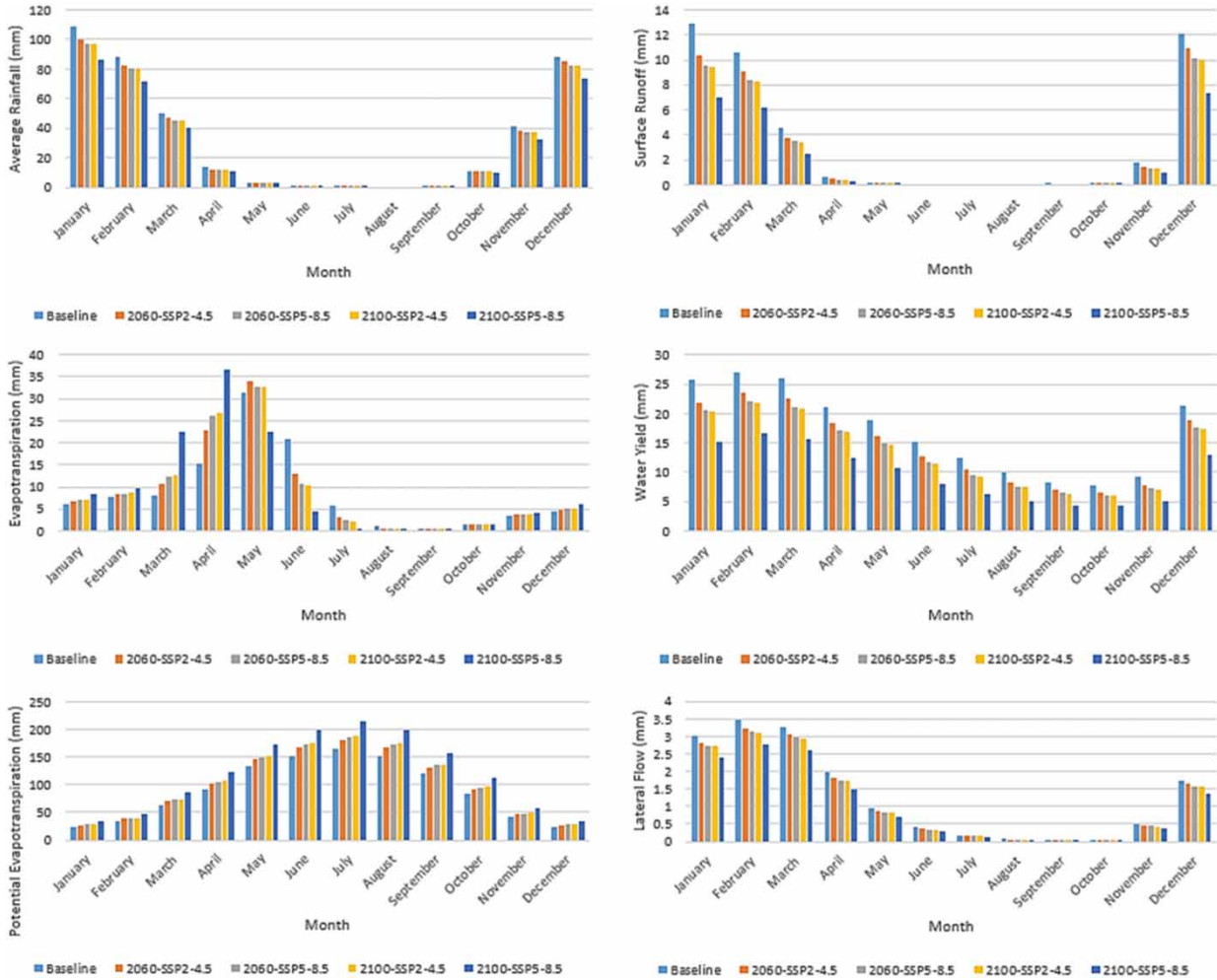

Figure 11 | Monthly averages of the hydrological elements in the Faria catchment.

Climate projections were derived from an ensemble of 23 GCMs under the SSP2-4.5 and SSP5-8.5 scenarios for 2060 and 2100. Under SSP5-8.5, groundwater recharge in sub-basin 8 declined by approximately 29.07% by 2100.

For comparison, a related study in the Gaza Strip employed the WetSPASS model to assess surface and soil water balance under the Fossil energy-intensive scenario (A1FI). Despite differences in model type, input data, and time periods, similar trends were observed: a 5.28 °C rise in temperature and a 14.56% decline in rainfall. This alignment reinforces the broader regional expectation of warming and drying.

The convergence of findings across modeling frameworks highlights the robustness of projected hydrological impacts and underscores the importance of refining baseline assumptions, improving data resolution, and enhancing calibration to support informed adaptation planning.

While using the median ensemble from 23 GCMs provides a representative central estimate, it does not capture the full range of potential future outcomes, highlighting the value of incorporating comprehensive uncertainty analyses in future studies to support more risk-informed water resource management strategies.

5. CONCLUSIONS

Future hydrological projections for the Faria catchment indicate intensifying water scarcity driven by climate change. By mid-century, under moderate emission scenarios, substantial declines in SRO coincide with rising ET rates. Under high-emission scenarios by the end of century, more reductions in runoff and groundwater recharge converge with amplified ET losses. These changes collectively diminish total water availability, disproportionately affecting high-elevation sub-basins where

reduced winter flows and intensified summer evaporation threaten rain-fed agricultural systems. Such hydrological shifts necessitate urgent reconfiguration of water allocation frameworks to safeguard aquifer integrity and farming livelihoods.

While the study provides robust insights into the hydrological impacts of climate change in the Faria catchment, certain limitations should be noted. Quantified uncertainty ranges were not incorporated, extreme climate events are only partially represented, and the SWAT model did not include a warm-up period. Interactions between groundwater and surface water were not fully captured, and additional bias-correction methods could improve climate input accuracy. Addressing these aspects in future studies, alongside exploring a wider set of climate scenarios such as SSP3-7.0, would further strengthen the reliability and policy relevance of the results, without undermining the robustness of the current findings.

To support adaptive water management, three priorities emerge: First, integrating dynamic land-use projections with hydrological models to quantify agricultural intensification feedbacks on water scarcity. Second, advancing sub-daily modeling frameworks to resolve ephemeral channel responses critical for flood infrastructure planning. Third, co-developing adaptation portfolios with water authorities prioritizing distributed rainwater harvesting, managed aquifer recharge in critical sub-basins, and ET-informed irrigation scheduling. Such place-based, data-guided strategies offer pathways to preserve the Faria catchment's vital role as the West Bank's agricultural cornerstone amidst hydroclimatic change.

DATA AVAILABILITY STATEMENT

All relevant data are included in the paper or its Supplementary Information.

CONFLICT OF INTEREST

The authors declare there is no conflict.

REFERENCES

Abbaspour, K. C. (2015) *SWAT-CUP-SWAT Calibration and Uncertainty Programs*. Dübendorf, Switzerland. Available at: https://swat.tamu.edu/media/114860/usermanual_swatcup.pdf.

Abboushi, A. (2013) *A Preliminary Investigation of Wadi-Aquifer Interaction in Semi-Arid Regions: The Case of Faria Catchment, Palestine*. An-Najah National University Nablus, Palestine. Available at: https://scholar.najah.edu/sites/default/files/Atta%20Abboushi.pdf.

Abedel-Kareem, S. (2005) *GIS-Based Hydrological Modeling of Semiarid Catchments (The Case of Faria Catchment)*. An-Najah National University Nablus, Palestine. Available at: https://staff-old.najah.edu/sites/default/files/GIS-Based_Hydrological_Modeling_of_Semiarid_Catchments_(The_Case_of_Faria_Catchment).pdf.

Abu Hijleh, R. J. (2014) *Chemical and Microbial Risk Assessment of Drinking Water in Faria Catchment.* An-Najah National University Nablus, Palestine. Available at: https://scholar.najah.edu/sites/default/files/Reem%20Abu%20Hijleh.pdf.

Arnold, J. G., Srinivasan, R., Muttiah, R. S. & Williams, J. R. (1998) Large area hydrologic modeling and assessment part I: model development, *Journal of the American Water Resources Association*, **34** (1), 73–89. https://doi.org/10.1111/j.1752-1688.1998.tb05961.x.

Arnold, J. G., Moriasi, D. N., Gassman, P. W., Abbaspour, K. C., White, M. J., Srinivasan, R., Santhi, C., Harmel, R. D., Van Griensven, A., Van Liew, M. W. & Kannan, N. (2012) SWAT: model use, calibration, and validation, *Transactions of the ASABE*, **55** (4), 1491–1508.

Falkenmark, M. & Rockström, J. (2006) The new blue and green water paradigm: breaking new ground for water resources planning and management, *Journal of Water Resources Planning and Management*, **132** (3), 129–132. https://doi.org/10.1061/(asce)0733-9496(2006)132:3(129).

Gleick, P. H. (1998) Water in crisis: paths to sustainable water use, *Ecological Applications*, **8** (3), 571–579. https://doi.org/10.1890/1051-0761(1998)008[0571:WICPTS]2.0.CO;2.

Haji, H. (2017) *Developing and Mapping Rainfall Intensity, Duration, and Frequency Curves in Al-Faria Catchment.* An-Najah National University Nablus, Palestine. Available at: https://repository.najah.edu/handle/20.500.11888/13228.

Hoekstra, A. Y. & Mekonnen, M. M. (2012) The water footprint of humanity, *Proceedings of the National Academy of Sciences*, **109** (9), 3232–3237. https://doi.org/10.1073/pnas.1109936109/-/DCSupplemental.

IPCC (2014) *Climate Change 2014: Synthesis Report.* Geneva, Switzerland: IPCC.

Jahanshahi, A., Golshan, M. & Afzali, A. (2017) Simulation of the catchments hydrological processes in arid, semi-arid and semi-humid areas, *Desert*, **22** (1), 1–10. https://doi.org/10.22059/jdesert.2017.62295.

Kim, K. B., Kwon, H. H. & Han, D. (2018) Exploration of warm-up period in conceptual hydrological modelling, *Journal of Hydrology*, **556**, 194–210. https://doi.org/10.1016/j.jhydrol.2017.11.015.

Legesse Gebre, S. (2015) Hydrological response to climate change of the upper Blue Nile River basin: based on IPCC Fifth Assessment Report (AR5), *Journal of Climatology & Weather Forecasting*, **03** (01), 1–15. https://doi.org/10.4172/2332-2594.1000121.

Masson-Delmotte, V., Zhai, P., Pirani, A., Connors, S. L., Péan, C., Berger, S., Caud, N., Chen, Y., Goldfarb, L., Gomis, M. I. & Huang, M. (2021) *Climate Change 2021: The Physical Science Basis.* IPCC. Cambridge University Press, Cambridge, United Kingdom and New York, NY, USA. Available at: www.ipcc.ch.

Mata, L. J., Arnell, N. & Doell, P. (2007) *Freshwater Resources and Their Management*. Cambridge University Press, Cambridge, United Kingdom and New York, NY, USA. Available at: https://www.researchgate.net/publication/263557304.

Mendoza, J. A. C., Alcazar, T. A. C. & Medina, S. A. Z. (2021) Calibration and uncertainty analysis for modelling runoff in the Tambo River Basin, Peru, using Sequential Uncertainty Fitting Ver-2 (SUFI-2) algorithm, *Air, Soil and Water Research*, **14**, 1178622120988707. https://doi.org/10.1177/1178622120988707.

Moriasi, D. N., Arnold, J. G., Van Liew, M. W., Bingner, R. L., Harmel, R. D. & Veith, T. L. (2007) Model evaluation guidelines for systematic quantification of accuracy in watershed simulations, *Transactions of the ASABE*, **50** (3), 885–900. https://doi.org/10.13031/2013.23153.

Neitsch, S. L., Arnold, J. G., Kiniry, J. R., Williams, J. R. & King, K. W. (2002) *Soil and Water Assessment Tool User's Manual – Version 2000*. Temple, Texas. Available at: https://swat.tamu.edu/media/1294/swatuserman.pdf (Accessed: 17 September 2025).

Neitsch, S. L., Arnold, J. G., Kiniry, J. R., Williams, J. R. & King, K. W. (2011) *Soil and Water Assessment Tool Theoretical Documentation Version 2009*. Temple, Texas.

Pérez-Sánchez, J., Senent-Aparicio, J., Segura-Méndez, F., Pulido-Velazquez, D. & Srinivasan, R. (2019) Evaluating hydrological models for deriving water resources in peninsular Spain, *Sustainability (Switzerland)*, **11** (10), 2872. https://doi.org/10.3390/su11102872.

Riahi, K., Van Vuuren, D. P., Kriegler, E., Edmonds, J., O'neill, B. C., Fujimori, S., Bauer, N., Calvin, K., Dellink, R., Fricko, O. & Lutz, W. (2017) The Shared Socioeconomic Pathways and their energy, land use, and greenhouse gas emissions implications: an overview, *Global Environmental Change*, **42**, 153–168. https://doi.org/10.1016/j.gloenvcha.2016.05.009.

Saade, J., Atieh, M., Ghanimeh, S. & Golmohammadi, G. (2021) Modeling impact of climate change on surface water availability using SWAT model in a semi-arid basin: case of El Kalb river, Lebanon, *Hydrology*, **8** (3), 134. https://doi.org/10.3390/HYDROLOGY8030134.

Santhi, C., Arnold, J. & Williams, J. (2001) *Validation of the Soil and Water Assessment Tool (SWAT) for a Large River Basin in Texas*. https://doi.org/10.1111/j.1752-1688.2001.tb03630.x

Schneider, T. & Novak, L. (2023) *Physics of Earth's Climate*. https://climate-dynamics.org/wp-content/uploads/2017/04/Climate_Book.pdf.

Shadeed, S. (2008) *Up to Date Hydrological Modeling in Arid and Semi-Arid Catchment, the Case of Faria Catchment, West Bank, Palestine. Doctoral dissertation*. Verlag nicht ermittelbar. Available at: https://www.researchgate.net/publication/29758002.

Shadeed, S., Jayyousi, A. & Shaheen, H. (2014) *Probability Distribution of Faria-Catchment Rainfall*. An-Najah National University Nablus, Palestine. Available at: https://www.researchgate.net/publication/267832918.

Shadeed, S., Sawalhah, M., Jaish, A. A., Haddad, M., Alawneh, A., Abboushi, A. & Homeidan, M. (2017) *Overview of Quantity and Quality of Water Resources in the Faria Catchment, Palestine*. An-Najah National University Nablus, Palestine. Available at: https://staff.najah.edu/media/conference/2017/04/12/Overview_of_Quantity_and_Quality_of_Water_Resources_in_the_Faria_Catchment_Palestine.pdf (Accessed: 17 September 2025).

Sulaiman, H. (2017) *Distributed Hydrological Modeling of Semi-Arid Regions: The Case of Al-Faria Catchment, West Bank, Palestine*. An-Najah National University Nablus, Palestine. Available at: https://repository.najah.edu/bitstream/20.500.11888/13185/1/Distributed-Hydrological-Modeling-of-Semi-Arid-Regions-the-Case-of-Al-Faria-Catchment-West-Bank-Palestin~0.pdf (Accessed: 18 January 2025).

Tebaldi, C., Debeire, K., Eyring, V., Fischer, E., Fyfe, J., Friedlingstein, P., Knutti, R., Lowe, J., O'Neill, B., Sanderson, B. & Van Vuuren, D. (2020) Climate model projections from the Scenario Model Intercomparison Project (ScenarioMIP) of CMIP6, *Earth System Dynamics*, **12** (1), 253–293. https://doi.org/10.5194/esd-2020-68.

Urich, P., Kouwenhoven, P. & Feras, K. (2014) New IPCC climate models released: understanding the planning implications for water resiliency, *Journal AWWA*, **106** (6), 51–60.

Vörösmarty, C. J., Green, P., Salisbury, J. & Lammers, R. B. (2000) Global water resources: vulnerability from climate change and population growth, *Science*, **289** (5477), 284–288. https://doi.org/10.1126/science.289.5477.284.

First received 28 May 2025; accepted in revised form 20 August 2025. Available online 25 September 2025